applied sciences

MDPI

Article

An Investigation on Mineral Dissolution and Precipitation in Cement-Stabilized Soils: Thermodynamic Modeling and Experimental Analysis

Enyue Ji [1,†], Fei Xu [2,*,†], Hua Wei [2], Wenxun Qian [2], Yang He [2] and Pengfei Zhu [2]

[1] Department of Geotechnical Engineering, Nanjing Hydraulic Research Institute, Nanjing 210029, China; eyji@nhri.cn
[2] Department of Materials and Structural Engineering, Nanjing Hydraulic Research Institute, Nanjing 210029, China; hwei@nhri.cn (H.W.); wxqian@nhri.cn (W.Q.); yhe@nhri.cn (Y.H.); pfzhu@nhri.cn (P.Z.)
* Correspondence: fxu@nhri.cn
† These authors contributed equally to this work.

Abstract: Thermodynamic modeling helps to reveal insights into the basic chemical kinetics of dissolution and precipitation in cementitious materials, but relevant applications to cement-stabilized soils have seldom been reported. Based on the thermodynamic database of Cemdata18 and the pore solution composition of cement-stabilized soils, this study formulated a specialized thermodynamic model, using essential thermodynamic constants for soil minerals that were calculated to ensure the model's accuracy. Two commercial admixtures of alkaline activator and polynaphthalene sulfonate were selected for the different modification mechanisms and plain and modified cement-stabilized soils were prepared. Compressive strength was tested to determine the specimens for pore solution analysis and the influences of the admixture type and dose on dissolution and precipitation were investigated by modeling the ionic activity products and saturation indexes. An X-ray diffraction (XRD) analysis was performed to verify and complement the thermodynamic results. The major research findings were that (1) thermodynamic modeling can be reliably applied to cement-stabilized soils by providing the essential thermodynamic data and an appropriate product model, (2) the pozzolanic reaction is accelerated by increasing the OH^- concentration in the pore solution, while the cement hydration is highly dependent on the dissolution of $Ca(OH)_2$ and the relevant complexes and (3) the dissolution equilibrium of $Ca(OH)_2$ is directly affected by the alkaline activator dissolution and is indirectly affected by the polynaphthalene sulfonate adsorption of the reactants.

Keywords: thermodynamic modeling; cement-stabilized soil; dissolution and precipitation; alkaline activator; polynaphthalene sulfonate

Citation: Ji, E.; Xu, F.; Wei, H.; Qian, W.; He, Y.; Zhu, P. An Investigation on Mineral Dissolution and Precipitation in Cement-Stabilized Soils: Thermodynamic Modeling and Experimental Analysis. *Appl. Sci.* **2022**, *12*, 6843. https://doi.org/10.3390/app12146843

Academic Editors: Qingbing Liu and Youkou Dong

Received: 4 June 2022
Accepted: 4 July 2022
Published: 6 July 2022

1. Introduction

Chemical treatment is a typical technique for soft soil stabilization in civil engineering and hydraulic scenarios, with cement being used as a common stabilizer [1]. The engineering performances, such as strength [2,3], compressibility [2] and durability [4], of stabilized soils can be significantly improved compared to natural soft soils by adding cement. The regulation and enhancement of these performances have become the major motivations for current research and applications, which, to the best knowledge of the authors, normally consist of (1) investigating the performance modification effects of different admixtures and (2) exploring the kinetics of performance development.

The admixtures for cement-stabilized soils are generally categorized as either mineral or chemical admixtures [5]. Fly ash [6], slag [7,8] and silica fume [9] are the typical mineral admixtures and their modification effects and corresponding mechanisms have long been investigated and are well clarified. Regarding chemical admixtures, one common type

comprises the alkaline activators R_2O–SiO_2, ROH, R_2SO_4, R_2CO_3 (R = K or Na or 0.5 Ca) and combinations of these [3,10–12]. It has been reported that the proper addition of alkaline activators not only causes an increase in the unconfined compressive strength (UCS), microstructural density, soil mineral pozzolanicity and the total amount of reaction products of cement-stabilized soils [3,11], but also a reduction in their compactibility [3,12,13]. Another common chemical admixture is the superplasticizer naphthalene [14–16], which produces similar influences on UCS, microstructural density and the total amount of reaction products as the alkaline activators, but it conversely influences the compactibility and pozzolanicity of the soil minerals. These reviewed studies have mainly attributed their experimental observations to the accelerated effects of chemical admixtures on the reaction progress within the system. Moreover, by combining knowledge from the cement industry, Xu et al. [15] proposed that the modification effects of naphthalene are derived from the inhomogeneous adsorption of superplasticizer molecules on the different components of cement-stabilized soils. Notably, the soil types have varied among the reviewed literature, but the corresponding impacts on the modification effects of the admixtures have not been fully considered. Meanwhile, some of the literature has reported that the UCS reductions in cement-stabilized soils are caused by the improper addition of both alkaline activators [3] and the naphthalene superplasticizer [17], but the reasons for this have not been clearly addressed.

Regarding the kinetics of performance development, it is widely accepted that cement-stabilized soils share the basic chemical mechanisms of dissolution and precipitation with cementitious materials, such as mortar and concrete [4,18–20]. Knowledge [21] from cementitious materials has stated that after contact with water, the clinkers initially dissolve to form supersaturated aqueous phases and the hydrates subsequently precipitate from the solution. Meanwhile, by formulating a thermodynamic model, the chemical states of the dissolution and precipitation of certain compositional minerals within cementitious materials can be quantified by the corresponding saturation level (i.e., saturation index, which is denoted as *SI*) with respect to the pore solution [20,22], which has provided profound insights into the multicomponent systems of cementitious materials. In addition to chemical state quantification, thermodynamic modeling has been successfully employed to predict the time-dependent phase assemblage of cementitious materials [20,23] and assess their interactions with the environment [20,24]. Though the thermodynamic method has been successfully applied to cementitious materials, it has not been systematically extrapolated to cement-stabilized soils. Some pioneer works have calculated the *SI* values the minerals ettringite (AFt) [6] and $Ca(OH)_2$ [25] with respect to different chemically stabilized soils, which has revealed the impacts of these two minerals on the engineering performances of the respective systems. However, the influence of the coexistence of complex aqueous species on *SI* calculations has not been considered in previous works and the evaluation of the general chemical processes of cement-stabilized soils using a single phase may not be accurate enough since some hydrated phases (such as $Ca(OH)_2$) are the reactants of the simultaneous pozzolanic reactions of soil minerals [26,27].

From the reviewed literature, it could be summarized that there is somewhat of a divergence in the modification effects of alkaline activators and superplasticizers on the performances of cement-stabilized soils, with the failure mechanisms and the influences of soil minerals remaining unclear. On the other hand, the current literature has normally investigated the modification mechanisms based on the observation and/or modeling of the characteristics of different scales but has suffered from a lack of analysis involving mineral dissolution and precipitation, which is a more fundamental perspective to be addressed by the thermodynamic method.

In view of the above, this study tried to formulate a relatively rigorous thermodynamic model for a given cement-stabilized soil to investigate the reactant dissolution and product precipitation, based on the mineralogy of the raw materials and the thermodynamic data. For the thermodynamic modeling, the pore solution composition was the input data, the modeling codes were computed on PHREEQC [28] coupled with the thermodynamic

database Cemdata18 [29] and the essential thermodynamic constants for the soil minerals were calculated. For the experimental analyses, two types of chemical admixtures, the modification effects of which have been documented in previous works [3,15], were added to the given plain cement-stabilized soil. The UCS values of the stabilized soil were tested to select appropriate specimens for the time-dependent pore solution extraction and the thermodynamic analysis. Then, the X-ray diffraction (XRD) patterns of the selected specimens were explored to validate and deepen the modeling analysis.

2. Materials

2.1. Cement, Water and Soil

Ordinary Portland cement (P·O 42.5) and distilled water were used in this study. A bentonite soil, which hydrates intensively and provides enormous amounts of exchangeable cations [30], was sampled near the Yangtze river in Nanjing, China. The soil was first oven-dried, then passed through a 2-mm sieve and tested for the geotechnical properties of liquid and plastic limits, compactibility and exchangeable cation value, controlling to ASTM D4318, D1557 and D7503, respectively. Then, it was ground to a particle size of $\leq$75 μm to determine the mineralogy using an XRD Rietveld with the code GSAS. The geotechnical properties and mineralogy of the soil are summarized in Table 1.

Table 1. The geotechnical properties and mineralogy of the soil.

Properties	Index	Value
Geotechnical Properties	Liquid Limit (%)	60.6
	Plastic Limit (%)	38.7
	Plasticity Index, PI	21.9
	Optimum Moisture Content (%)	34.8
	Maximum Dry Density (g/cm^3)	1.65
	Exchangeable Cation Amounts (meq/100 g)	
	Na^+	27.6
	K^+	3.1
	Ca^{2+}	9.7
Mineralogy	Quartz (%)	28
	Montmorillonite (%)	46
	Muscovite (%)	17
	Albite (%)	7

2.2. Admixtures

A commercial composite alkaline activator and sodium polynaphthalene sulfonate, which were purchased from Nanjing R&D Hightech Company Limited (Nanjing, China), were used as the admixtures and were denoted as JA and PNS, respectively. JA was a mixture of aluminates and sulfates and its chemical composition was determined using a SHIMADZU (Kyoto, Japan) X-ray fluorescence spectrometer XRF-1800, with Na_2O = 12.2%, CaO = 24.8%, Al_2O_3 = 54.5% and SO_3 = 8.5%. The pH of the JA solution was 12.5, with a solid:liquid ratio of 1:10. The PNS, as a typical water-reducing agent in concrete with a water-reducing rate of 15%, had functional groups of sulfonate, hydroxyl, alkane and naphthalene [15]. The pH of the PNS solution was 9.4, with a solid:liquid ratio of 1:10.

3. Thermodynamic Modeling

3.1. Modeling Basis

This study used the code PHREEQC to compute the model, which quantified the equilibrium state of the reaction products using *SI*, with $SI < 0$ corresponding to mineral dissolution (undersaturation) and $SI > 0$ corresponding to mineral precipitation (supersaturation) [31]. The input data for the model calculation were the pore solution

compositions of the selected cement-stabilized soils. *SI* was calculated from the ion activity product (*IAP*) and the equilibrium constant (K_{eq}) of the phase using Equation (1) [32]:

$$SI = \lg \frac{IAP}{K_{eq}} \quad (1)$$

For a given dissolution reaction $A_2B \rightarrow 2A^+ + B^{2-}$, the *IAP* of A_2B was obtained from Equation (2):

$$IAP = \frac{[A^+]^2 \cdot [B^{2-}]}{[A_2B]^0} \quad (2)$$

where A^+, B^{2-} and A_2B correspond to the activities of the aqueous species A^+, B^{2-} and A_2B, respectively. The activity *i* of any specie *i* was calculated using Equation (3):

$$[\, i \,] = m_i \gamma_i \quad (3)$$

where m_i is the mass molar concentration of ion *i* (mol/kg) and γ_i is the activity coefficient of ion *i*, which was calculated with the well-known Debye–Hückel equation [33].

Notably, Equation (2) suggested that the higher the dissolution magnitude of A_2B, the higher the *IAP* value. Thus, the index lg*IAP* was used in this study to evaluate the dissolution magnitude of the reactants, following the conventions of cement chemistry and geochemistry [29].

3.2. Maintenance of Thermodynamic Database

Modeling reliability is largely dependent on one aspect: the accuracy and completeness of the thermodynamic properties of the species involved in the system, which are normally acquired from a thermodynamic database. The thermodynamic database Cemdata18 [29] was used for the modeling in this study. For the systems of the cement-stabilized soils, this study assumed that the dissolution processes of different types of reactants did not interfere with each other, but rather that they were controlled by the saturation of the compositional ions within the pore solution. The reaction products of the cement-stabilized soil systems were mainly composed of the cement hydrates and pozzolanic products of the soil minerals and the systems were abundant in aluminosilicates but scarce in calcium. Thus, in terms of hydrate precipitation, this study used siliceous hydrogarnet [29] and a C-(N-)A-S-H solid solution [29] to simulate the uptake of silica in hydrogarnet and aluminum and the reduction in sodium in Ca/Si CSH, respectively. Regarding the pozzolanic products, this study introduced typical sodium- and calcium-based zeolites, including natrolite, chabazite and gismondine, which were input into Cemdata18 on the basis of the previous literature [34,35].

The thermodynamic data for the reactants montmorillonite, albite and muscovite are not recorded in Cemdata18. Hence, this study calculated the K_{eq} values using the relationship (Equation (4)) between the Gibbs free energy of the reaction (ΔG_r^0) and the K_{eq} for any reaction that reached chemical equilibrium and the corresponding dissolution equations and the estimation method for the Gibbs free energy of the formation ($\Delta_f G^0$) of layered silicates, as proposed by Tardy et al. [36].

$$-\Delta G_r^0 = \sum \Delta_f G^0_{reatants} - \sum \Delta_f G^0_{products} = RT \ln K_{eq} \quad (4)$$

where $\Sigma \Delta_f G^0_{reactants}$ and $\Sigma \Delta_f G^0_{products}$ correspond to the total Gibbs free energy of the formation of the reactants and products, respectively, R = 8.31451 J/(mol·K) is the universal gas constant and *T* is the temperature in Kelvin.

The dissolution equations and calculated K_{eq} values of montmorillonite, albite and muscovite are summarized in Table 2. According to the CEC analysis in Table 1, sodium-based montmorillonite (Na montmorillonite) and sodium-based albite (Na albite) were used in the modeling.

Table 2. The K_{eq} values of the soil minerals.

Mineral	Reaction	K_{eq}
Na montmorillonite	$Na_{0.33}Al_{2.33}Si_{3.67}O_{10}(OH)_2 + 2OH^- + 7.34H_2O = 0.33Na^+ + 2.33Al(OH)_4^- + 3.67H_4SiO_4$	$10^{21.86}$
Muscovite	$KAl_3Si_3O_{10}(OH)_2 + 10H_2O + 2OH^- = K^+ + 3Al(OH)_4^- + 3H_4SiO_4$	0.794
Na albite	$Na(AlSi_3O_8) + 8H_2O = Na^+ + Al(OH)_4^- + 3H_4SiO_4$	$10^{-18.00}$

The standard temperature of 25 °C in Cemdata18 is higher than the curing temperature of this study (20 °C). Therefore, the K_{eq} values of the related ions and minerals at 20 °C were calibrated according to Equation (5) [32]:

$$\ln K_{eq} = \ln K_{eq,25^\circ C} + \frac{\Delta H}{R}\left(\frac{1}{298.15} - \frac{1}{T}\right) \quad (5)$$

where ΔH corresponds to the standard enthalpy change, which was provided by Cemdata18.

4. Experimental Procedure

4.1. Specimen Preparation

The mixture proportions and the corresponding specimen names are summarized in Table 3. Controlling to ASTM D1557, the maximum dry density and the optimum water content of the plain cement-stabilized soil were 1.58 g/cm^3 and 35.7%, respectively. Thus, all specimens were prepared using the static pressure method with a cubic die of 70.7 mm, a dry density of 1.55 g/cm^3 and a moisture content of 35%, which aimed to alleviate the disturbances from physical factors. The curing conditions were controlled to 20 °C and an RH of 95%.

Table 3. The mixture proportions (%) and specimen names.

Soil	Cement	JA Dose	PNS Dose	Specimen Name
90	10	\	\	CS *
90	10	0.4	\	JA4
90	10	0.6	\	JA6
90	10	0.8	\	JA8
90	10	1.0	\	JA10
90	10	1.2	\	JA12
90	10	\	0.06	PNS6
90	10	\	0.09	PNS9
90	10	\	0.12	PNS12
90	10	\	0.15	PNS15
90	10	\	0.18	PNS18

* the control sample of the plain cement-stabilized soil.

4.2. Pore Solution Separation and Analysis

The pore solution separation and analysis were conducted to provide the essential input data for the thermodynamic model. The pore solution was separated using a steel die under high pressure. The separation was carried out in a press machine with a pressure loading rate of 0.2 kN/s and a maximum pressure of 300 kN. The pore solution was first collected with a disposable needle and then subjected to centrifugation and filtration. The OH^- concentration in the pore solution was titrated, the SO_4^{2-} concentration was determined using an ICS-1100 ion chromatograph and the concentrations of Na, K, Ca, Al and Si were determined using an Agilent (Santa Clara, CA, USA) 5110 that was inductively coupled with a plasma emission spectrometer (ICP-OES). Then, the activities of the aqueous species were automatically determined using their corresponding K_{eq} values and PHREEQC. A graphic abstract of the aforementioned procedure is presented in Figure 1.

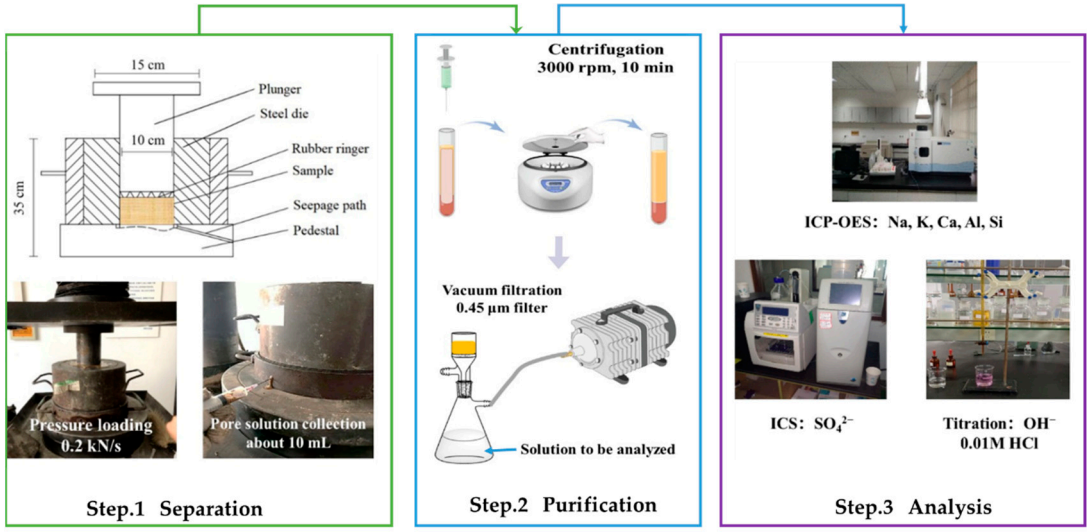

Figure 1. A graphic abstract of the pore solution analysis.

4.3. XRD Test

The specimen mineralogy was analyzed using the XRD technique, which was performed to verify the correctness of the thermodynamic modeling and was conducted on a Rigaku (Tokyo, Japan) SmartLab X-ray diffractometer with Cu(Kα) radiation (wavelength = 0.154 nm). The scanning voltage, current and speed were 40 kV, 40 mA and 5 °/min, respectively.

5. Results and Discussion

5.1. UCS Analysis

Figure 2a,b compare the UCS values of the JA group to the CS specimen and those of the PNS group to the CS specimen, respectively.

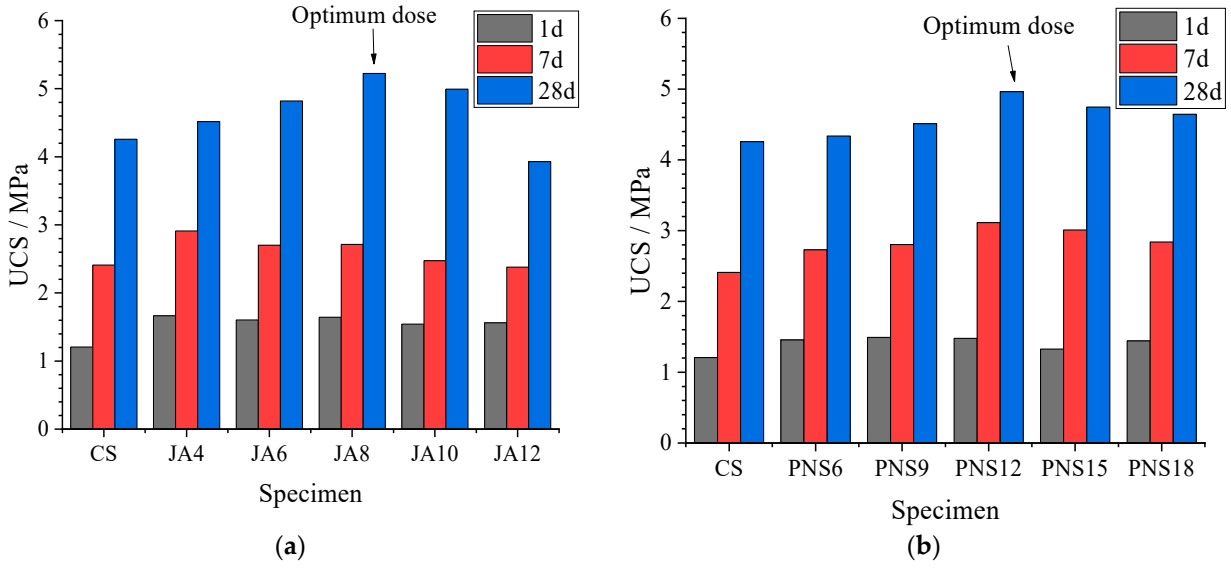

Figure 2. A summary of the UCS development in JA (**a**) and PNS (**b**).

It was clear that the UCS values of the cement-stabilized soils first increased and then reduced with the increased JA and PNS doses, with the optimum dose being 0.8% and 1.2%, respectively. The UCS values after 24 h, 168 h and 672 h increased by 138%, 118% and 123% using a JA dose of 0.8% and by 122%, 126% and 117% using a PNS dose of 1.2%,

respectively. However, compared to the CS specimen, the excessive JA dose (1.2%) caused substantial reductions in the UCS values after 168 h and 672 h, while high PNS doses only weakened the enhancement effects on the UCS values. These results indicated that the compressive strength of the cement-stabilized soils was influenced more significantly by the dose effects of JA than those of PNS due to the distinct modification mechanisms of the selected admixtures. Hence, thermodynamic modeling was conducted on the CS, JA8 and PNS12 specimens to investigate the improvement mechanisms of JA and PNS and on the JA12 and PNS18 specimens to investigate the modification mechanisms of excessive doses.

5.2. Pore Solution Analysis

The pore solution compositions of the selected specimens within the timeframe of 5 h–672 h are summarized in Table 4.

Table 4. The pore solution composition (mmol/kg) of the selected specimens.

Curing Period	Na + K	Na	Si	Al	Ca	SO_4^{2-}	OH^-
CS (no admixture)							
5 h	8.53	6.43	5.04	0.04	20.75	17.19	12.59
10 h	14.96	11.45	9.43	1.31	41.23	24.20	31.62
24 h	15.55	11.81	3.52	0.74	19.68	9.12	21.38
168 h	15.75	11.67	2.20	0.11	6.91	0.38	16.98
672 h	13.46	10.00	2.16	0.046	5.90	0.55	14.79
JA8 (JA dose = 0.8%)							
5 h	30.73	26.00	7.91	0.42	25.02	20.94	37.15
10 h	38.08	33.12	14.55	2.82	56.52	47.11	89.13
24 h	41.07	35.32	10.61	1.76	30.14	16.95	51.29
168 h	21.46	14.42	5.07	1.03	14.92	3.38	33.88
672 h	18.43	12.54	2.97	0.32	8.78	1.37	27.54
JA12 (JA dose = 1.2%)							
5 h	49.02	48.26	6.73	0.77	5.10	14.32	81.28
10 h	79.49	78.36	12.02	3.05	7.24	36.24	138.04
24 h	91.73	90.15	13.82	2.64	2.94	14.43	117.49
168 h	83.78	81.62	9.45	1.41	1.17	2.07	95.50
672 h	37.65	35.16	4.05	0.84	0.85	1.80	72.44
PNS12 (PNS dose = 1.2%)							
5 h	12.51	12.09	2.86	0.05	22.63	18.61	39.81
10 h	15.96	15.02	12.83	1.98	53.02	36.47	67.61
24 h	16.05	14.90	5.13	1.44	29.79	20.97	57.54
168 h	12.61	11.28	3.11	0.39	12.38	2.59	35.48
672 h	8.57	7.65	2.49	0.12	7.19	0.79	30.90
PNS18 (PNS dose = 1.8%)							
5 h	15.37	14.70	2.32	0.02	19.38	18.89	45.20
10 h	17.92	16.96	10.80	0.83	48.83	44.11	78.98
24 h	19.98	19.12	4.22	0.35	24.59	27.26	77.15
168 h	13.53	12.76	2.71	0.081	10.79	2.10	58.18
672 h	10.99	10.81	1.89	0.027	6.69	0.48	40.12

Table 4 indicates that the concentrations of all aqueous species first underwent an increase and then a subsequent reduction of different magnitudes with the increasing curing period. The concentration of Na + K peaked at 168 h in the CS specimen and at 24 h in the JA8, JA12, PNS12 and PNS18specimens, while the highest concentrations of the other aqueous species occurred at 10 h. The concentration increases in the early stages were mainly attributed to the reactant dissolution (Equations (6)–(8)), while the prolonged concentration increase in Na + K was due to the cation exchange reaction between the Ca^{2+} that was released from the clinker dissolution and the exchangeable Na^+ and K^+ in the soil minerals (in Equation (9), $\Theta|$ refers to a single soil mineral and M = Na or K). Then, the precipitation of the cement hydrates (Equation (10)) and the pozzolanic reaction products

(Equation (11)) continuously consumed the aqueous species, thereby reducing the total concentration of Na + K.

$$Na_{0.33}Al_{2.33}Si_{3.67}O_{10}(OH)_2 + 2OH^- + 7.34H_2O \rightarrow 0.33Na^+ + 2.33Al(OH)_4^- + 3.67H_4SiO_4 \quad (6)$$

$$CA + aH_2O \rightarrow xCa^{2+} + yNa^+ + zOH^- + wSO_4^{2-} + nAl(OH)_4^- \quad (7)$$

$$C_3S + C_2S + C_3A + 11H_2O \rightarrow 8Ca^{2+} + 10OH^- + 2H_2SiO_4^{2-} + 2Al(OH)_4^- \quad (8)$$

$$\Theta\left|\begin{matrix}M\\M\end{matrix}\right. + Ca^{2+} \rightarrow \Theta|Ca + 2M^+ \quad (9)$$

$$5Ca^{2+} + 6OH^- + 2Al(OH)_4^- + H_2SiO_4^{2-} \rightarrow CSH + CAH + Ca(OH)_2 \quad (10)$$

$$5M(OH)_2 + 2Al(OH)_4^- + 4H_bSiO_4^{b-4} \rightarrow MASH \quad (11)$$

Compared to the CS specimen, the addition of JA at a dose of 0.8% significantly improved the concentrations of all aqueous species, which was partly attributed to the accelerated dissolution of the cement clinkers [37] and the soil minerals [38] by the appropriately increased pH value. According to Equation (7), another reason for the concentration increases in Na + K, Al, Ca, SO_4^{2-} and OH^- was the JA dissolution. When the JA dose was increased to 1.2%, the concentrations of Na, Al and OH^- further increased, but the increases in the Si and SO_4^{2-} concentrations were lowered and the concentrations of Ca and K reduced to lower than those in the CS specimen. These results were related to the solubility of the ions in the pore solution and the compositional minerals of JA. As JA was composed of several minerals, the soluble minerals with smaller component ionic radii (e.g., Na^+ and OH^-) dissolved preferentially, thus limiting the dissolution of minerals with larger component ionic radii in either the JA or the raw materials (e.g., C_3S and C_3A in the clinkers). Furthermore, the reduced Ca concentration weakened the cation exchange reaction (Equation (10)), thereby lowering the K concentration. Meanwhile, the promotion effects of the high OH^- concentration in the soil mineral dissolution still existed and, therefore, maintained Si and Al concentrations at high magnitudes.

Regarding the PNS effects, Table 4 reveals that the optimum dose of 1.2% showed weaker effects on the concentration growth of Na, Si, Al, Ca, SO_4^{2-} and OH^- and resulted in a reduction in the concentration of K. When the PNS dose was increased to 1.8%, the K concentration continued to reduce and the concentrations of Na, SO_4^{2-} and OH^- further increased due to the PNS dissolution, but the promotion effects of PNS on the concentration growth of Si and Ca were weakened. Previous studies [39,40] have noted that the modification effects of PNS on cementitious materials are derived from the adsorption of PNS molecules on the particle surface and that the PNS molecules adsorb inhomogeneously in different clinkers, mainly due to electrostatic interactions. Hence, the authors suggest that the effects of the PNS addition on the pore solution composition of the cement-stabilized soils were related to the inhomogeneous adsorption of PNS in the different compositional minerals of the soil and cement.

5.3. Modeling Results and Analysis

5.3.1. Influences of the Admixtures on the Chemical States of the Compositional Minerals

With the pore solution data, the modeling results were calculated. The compositional minerals within the cement-stabilized soils were fully considered in the current thermodynamic model. To simplify the analyses, montmorillonite and C_3S were used to represent the reactants in the mineralogy of the raw materials, CSH and AFt were used to represent the cement hydrates in the crystallinity and fractions of the hydrates and natrolite was used to represent the pozzolanic products since Na^+ is the most abundant of the exchangeable cations in soil. The lg*IAP* values for the reactants montmorillonite and C_3S, from 5 h to 672 h, are summarized in Figure 3a,b, respectively. The *SI* values for the products CSH, AFt and natrolite are summarized in Figure 3c–e, respectively.

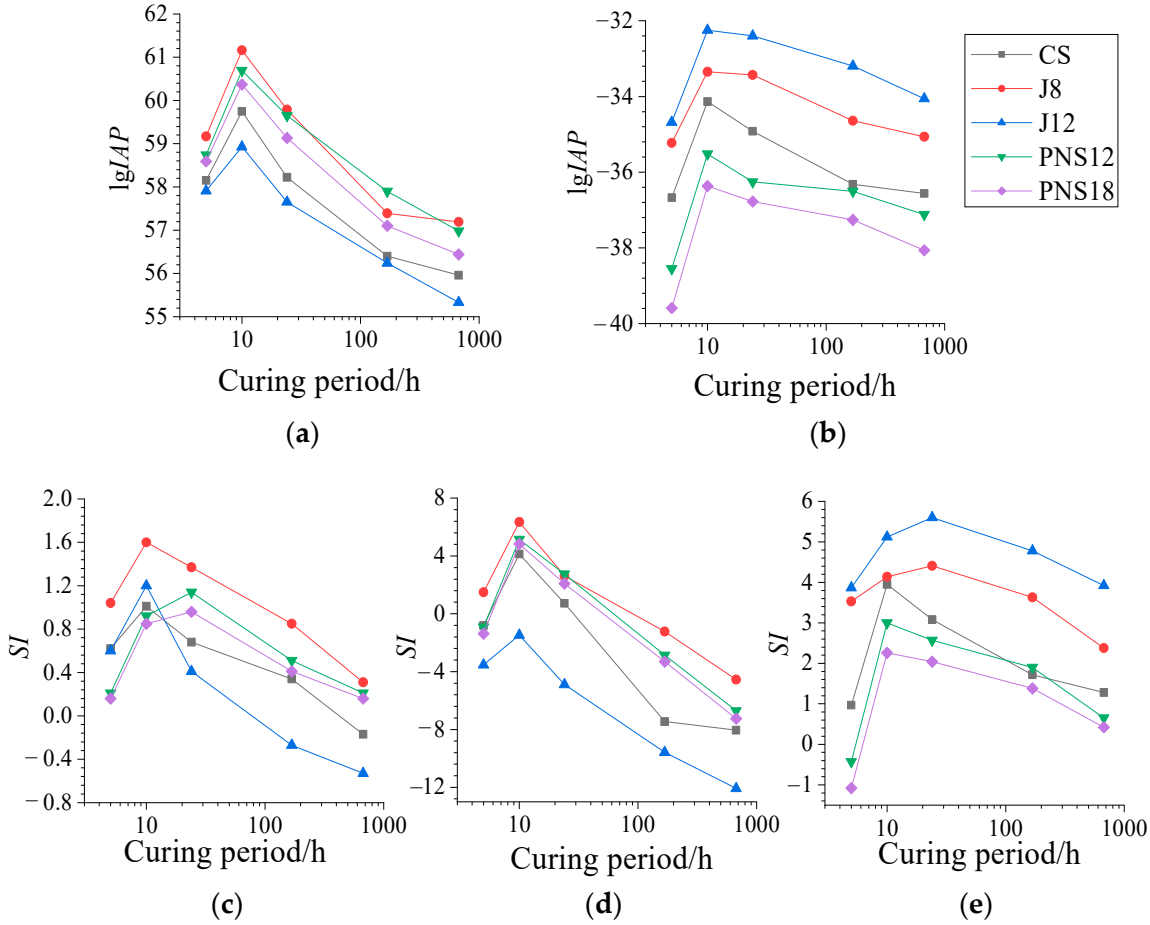

Figure 3. The thermodynamic calculations for the investigated minerals: (**a**) C3S; (**b**) montmorillonite; (**c**) C(N)ASH; (**d**) AFt; (**e**) natrolite.

Figure 3 shows that the development patterns of the reactant dissolution and product formation over the curing period were similar to those of the pore solution (as shown in Table 4), which confirmed that the chemical kinetics in the cement-stabilized soils was dominated by the dissolution and precipitation processes [21]. Due to the differences in solubility and mass fractions, the development patterns of the minerals that related to the pozzolanic reaction were significantly different from those relating to cement hydration. As montmorillonite had a lower solubility than C_3S, its lg*IAP* values were lower than those of C_3S; however, as montmorillonite was the most abundant mineral in the raw materials, its lg*IAP* values at 672 h were still higher than those at 5 h, while the lg*IAP* values of C_3S dropped below the initial values as early as after 168 h. The *SI* development of CSH, AFt and natrolite over the curing period indicated that the cement hydrates formed intensively before 10 h and turned out to be slowly formed or unstable in the long term, while the pozzolanic products formed stably and significantly affected the long-term performances of the cement-stabilized soils. Meanwhile, out of the investigated reaction products, only CSH produced a consistent pattern for UCS with respect to the type and dose of the admixtures. These results agreed well with the widely accepted knowledge [41] that the dominant chemical kinetics of the performance development of cement-stabilized soils are cement hydration, followed by the pozzolanic reaction of the soil minerals and that the crucial product that influences this performance is CSH. In addition, the change timing of the dominant chemical kinetics in the plain cement-stabilized soils was at around 168 h, which coincided with the first occurrences of CSH equilibrium and AFt undersaturation.

Regarding the individual effects of JA on the investigated minerals, the dose of 0.8% promoted the dissolution of C_3S and montmorillonite and affected the saturation levels of

CSH, AFt and natrolite to different magnitudes. The CSH formation was prolonged to after 672 h, the AFt dissolution after 168 h was inhibited and the timing of the highest *SI* value of natrolite was delayed to 24 h. When the JA dose was increased to 1.2%, the montmorillonite dissolution and natrolite supersaturation were further improved. While the C_3S dissolution was obviously inhibited, the first occurrence of CSH undersaturation was brought forward to 168 h and the AFt was lowered to an unsaturated level within the whole timeframe. Combining the analyses of the UCS and the pore solution, the modification effects of JA on the cement-stabilized soils were mainly derived from the dissolution process of the JA itself, which altered the alkalinity of the pore solution and affected the dissolution of the raw reactants within the system. By adding proper doses to the cement-stabilized soils, the increased alkalinity accelerated the reactant dissolution, thereby promoting the formation of cement hydrates and pozzolanic products and thus improving the UCS performance. In the case of excessive doses, the further increased alkalinity promoted the dissolution of the soil minerals and the formation of the pozzolanic products, but the dissolution of the calcium-based clinkers was inhibited due to the excessively dissolved ions with smaller radii (Table 4), thereby limiting the hydrate formation and the growth of UCS. These facts aligned with the previous knowledge [1,42] that the performances of cement-stabilized soils are highly dependent on the total amount of CSH. Note that the supersaturation level of CSH in the JA12 specimen still exceeded that in the CS specimen within 10 h. This phenomenon was due to the acceleration effects of the high alkalinity on the reactant dissolution, during which the pore solution was unsaturated in the very early stages of the reaction.

Regarding the effects of PNS, it was clear that increasing the dose substantially inhibited montmorillonite dissolution and natrolite formation, with natrolite becoming unsaturated at 5 h. This fact was ascribed to the hydrophobic layer that was generated by the adsorbed PNS molecules on the montmorillonite [15]. The overall dissolution of C_3S and the saturation levels of CSH and AFt were increased by the PNS addition, but the increments first increased and then decreased as the PNS dose increased from 1.2% to 1.8%. This result indicated the preferential adsorption of PNS on montmorillonite over the clinkers, which first retarded the pozzolanic reaction of montmorillonite and then the cement hydration. Notably, the early saturation levels of CSH and AFt were reduced by adding PNS due to the adsorbed PNS molecules on the clinker surfaces.

5.3.2. The Correlation Analysis of the Saturation Levels between $Ca(OH)_2$ and the Investigated Products

Figure 4 shows the correlation between the *SI* values of $Ca(OH)_2$ and those of CSH, AFt and natrolite since the saturation level of $Ca(OH)_2$ with respect to the pore solution was regarded as an indicator for the hydration rate of the clinkers [43].

The correlational analysis showed that the *SI* values of CSH and AFt grew linearly with those of $Ca(OH)_2$, indicating that the cement hydration was promoted by the increasing $Ca(OH)_2$ saturation within the pore solution. However, the R^2 of CSH was relatively low due to the uptake of aluminum and sodium in the low Ca/Si CSH. The saturation levels of natrolite were poorly correlated with those of $Ca(OH)_2$, with the *SI* value of natrolite having a positive proportional relationship with those of the JA series and PNS series. This fact was ascribed to the distinguished modification mechanisms of JA and PNS in the dissolution of the soil minerals, which were clarified by the above analyses. Considering that the permanent negative layer charge of soil minerals can consume the Ca^{2+} and $CaOH^+$ that is released by the clinker dissolution, the correlation analysis further suggested that the $Ca(OH)_2$ saturation was directly altered by the JA dissolution and was indirectly altered by the adsorption layer of PNS on the soil mineral surfaces.

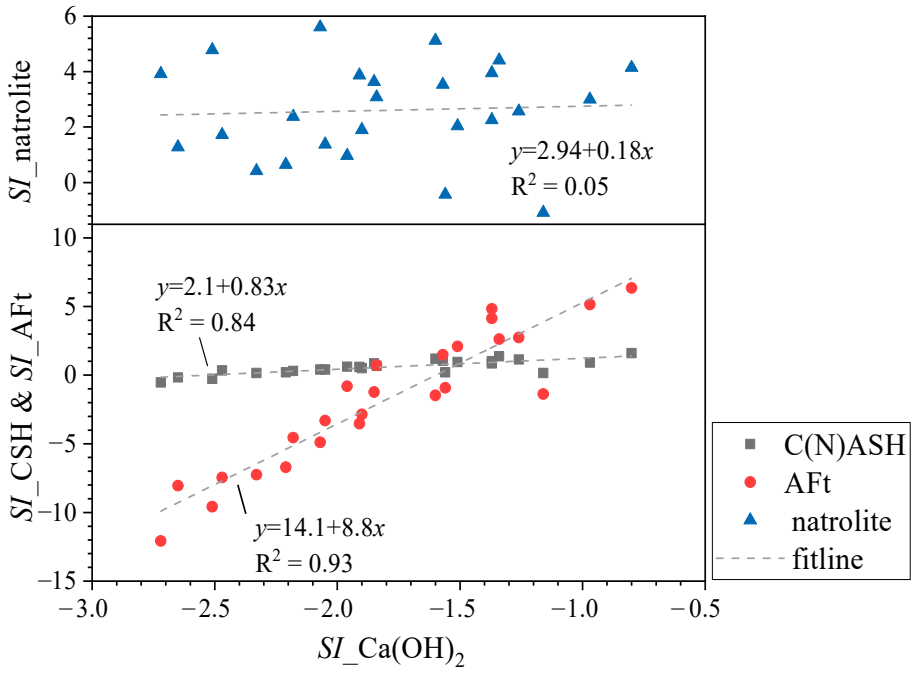

Figure 4. The correlation analysis of the *SI* values of $Ca(OH)_2$ and those of CSH, AFt and natrolite.

It is worth mentioning that the highest $Ca(OH)_2$ *SI* was −0.8, while under the same cement addition conditions, Yu et al. [25] detected supersaturated $Ca(OH)_2$ in cement-stabilized soils with low cation exchange capacities (≤32 meq/100 g), which had a higher strength than those with undersaturated $Ca(OH)_2$ and high cation exchange capacities. Hence, the authors suggest that the cation exchange process of the soil minerals was primarily ascribed to the undersaturation of $Ca(OH)_2$ and the slow strength increase in the cement-stabilized soils. In addition, the saturation level of $CaOH^+$ was investigated with respect to the thermodynamic equation $CaOH^+ \rightarrow Ca^{2+} + OH^-$, with *SI* values that fluctuated between 0.306 and 0.439 and a development pattern that was identical to that of $Ca(OH)_2$. This result suggested that the aqueous species of Ca, which should have crystallized to $Ca(OH)_2$, participated in the subsequent reactions in the form of $CaOH^+$.

5.4. Mineralogy Analysis and Validation

Figure 5 summarizes the XRD patterns of the specimens that were involved in the thermodynamic model and the two additional JA4 and PNS6 specimens. The XRD patterns of the specimens from the JA series and PNS series are presented in Figure 5a,b, respectively, and a detailed diagram of the 2θ range 27.8°–30.0° is shown in Figure 5a. The curing period was fixed to 168 h due to the thermodynamic analysis revealing that the investigated reaction products tended to precipitate in most of the specimens prior to this time.

The XRD patterns revealed that the reactants and products of the modified specimens were basically the same as the CS specimen, but the reflection intensity was altered by the admixture type and dose. The reactants that were detected by the X-ray diffractometer were the soil minerals within the raw materials, with the clinkers being undetectable due to the relatively high hydration rate. The common products that were detected in all patterns included CSH, AFt, gismondine and Na zeolite. Meanwhile, the reaction products CSH and Na zeolite also produced humps within the approximate 2θ range of 30–34° [44,45] in every pattern, which were the major diffraction characteristics of those minerals. Notably, the Na zeolite in this study was composed of natrolite and faujasite Na.

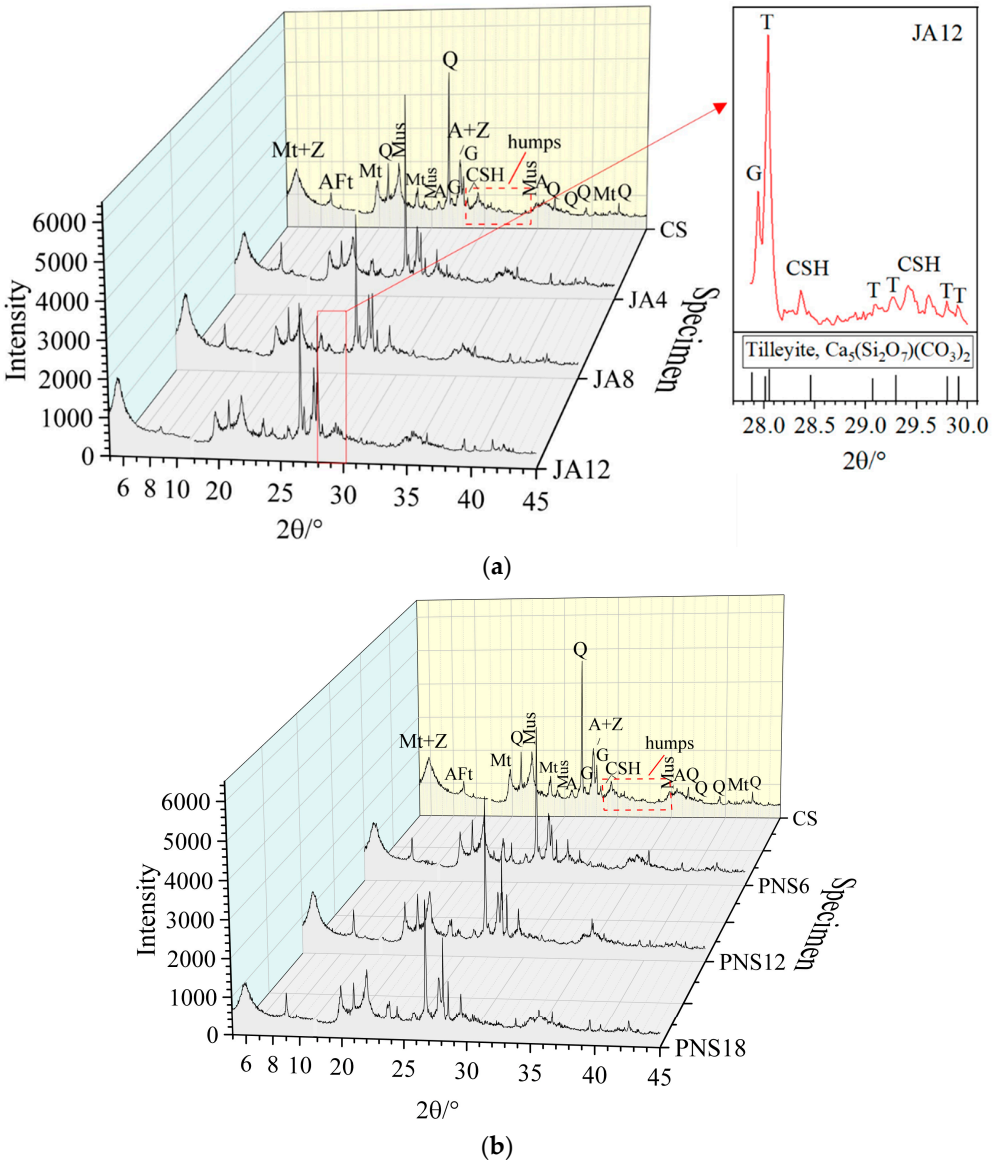

Figure 5. The XRD patterns of the specimens after 168 h: CS and the JA series (**a**) and CS and the PNS series (**b**). Mt, montmorillonite; Mus, muscovite; Q, quartz; A, albite; AFt, ettringite; Z, Na zeolite; G, gismondine; CSH, calcium silicate hydrate; T, tilleyite.

The modification effects of the admixtures on the cement hydrates that were revealed by the XRD technique coincided with those that were revealed by the *SI* analyses. In terms of CSH, limited information was provided by the intensity change of the humps due to its highly amorphous nature. Nevertheless, except for the JA dose of 1.2%, the addition of the admixtures improved the reflection intensity of CSH at around 28.3° and 29.4° compared to the CS specimen (to different magnitudes), with the improvements from the PNS doses of 1.2% and 1.8% exceeding those from the JA doses of 0.4% and 0.8%. The refection intensity of gismondine at 27.9° gave rise to a similar change pattern as that for CSH, implying that gismondine shared some reactants with CSH. Notably, a detailed diagram for the JA12 specimen showed that the reflection intensities of CSH and gismondine were substantially reduced by an excessive dose of JA and that a CO_2-containing silicate of tilleyite ($Ca_5Si_2O_7(CO_3)_2$) was formed. McDonald et al. [46] addressed the fact that CO_2-containing silicates (such as tilleyite), of which the cementing strength is relatively low, are the preferentially stable phase of calcium silicates under the coupled conditions of CO_2 presence and insufficient $Ca(OH)_2$. With this finding, our detailed diagram suggested that

the excessively high alkalinity of the pore solution led to the carbonation of the clinkers, thereby decreasing the compressive strength of the specimen [47,48].

Compared to CSH, the admixture addition produced a more prominent intensity change in the reflection of AFt. The intensity of the AFt reflection was 1066 in the CS specimen and a JA dose of 0.4% produced the highest intensity of the AFt reflection (1533), while the optimum JA dose (0.8%) produced a reflection intensity of 1300 and the excessive dose (1.2%) reduced the intensity to 802, which was lower than that of the CS specimen. The PNS doses of 0.6%, 1.2% and 1.8% produced reflection intensities of 1258, 1223 and 1153, respectively. The dose effects of PNS were similar to those of JA, but the inhibition of AFt formation did not occur. The peak intensity of AFt occurred at low doses in both the JA and PNS series. These results were attributed to the suitable pH for AFt formation being lower than that for CSH [43] in the JA series, while the adsorption of PNS molecules on calcium aluminates was superior to calcium silicates [49] in the PNS series. Additionally, according to the *SI* analysis (Figure 3d), AFt could hardly precipitate in JA12 at 5 h and the subsequent stages and the AFt reflection was detected in the XRD pattern of JA12 due to AFt being rapidly precipitated within the first hours of cement hydration.

Regarding the soil minerals and pozzolanic products, increasing the JA dose reduced the reflection intensity of the soil minerals, such as montmorillonite at 19.9° and muscovite at 21.9°, and increased the intensity of the superposition reflection of Mt + Z and A + Z. As shown by the *SI* analyses, these facts were induced by the promotion effects of the high alkalinity of the pore solution in the pozzolanic reaction. Compared to the JA series specimens, the corresponding reflections of the soil minerals were little affected by the addition of PNS, with the reflections of Mt + Z and A + Z being lower than those in the CS specimen. These results coincided with the *SI* analyses in general, but the dose effects of PNS on reflection intensity could not be quantified.

5.5. Discussion on the Analytical Features of Thermodynamic Modeling and XRD

As previously discussed, the saturation development of the investigated minerals that was revealed by the thermodynamic modeling showed good consistency with the XRD characterizations, thereby confirming the correctness of the model. Comparatively, the thermodynamic modeling provided direct information about the chemical states of the compositional minerals in the cement-stabilized soils, while the XRD provided indirect information about the changes in the diffraction intensities, which were related to the mineral mass fractions within the system. In addition, the thermodynamic modeling made up for the deficiencies in the XRD technique for mineral quantity characterization. For instance, this study was unable to characterize the development of the pozzolanic products from the PNS doses using XRD and the intensity changes that related to the effects of JA on AFt formation were not significant enough. Nevertheless, unexpected minerals (e.g., tilleyite) could be identified more easily using the XRD technique but could be neglected by the thermodynamic modeling due to the insufficiently comprehensive investigation into the aqueous species within the pore solution.

6. Conclusions

With respect to cement-stabilized soil systems, this study formulated a combined microscopic analyzing method, based on thermodynamic modeling and the XRD technique, so as to further clarify the modification mechanisms of a commercial composite alkaline activator (JA) and sodium polynaphthalene sulfonate (PNS) on the dissolution and precipitation of reactants and products. The feasibility and advantages of applying thermodynamic modeling to cement-stabilized soil systems were discussed, with the main conclusions being the following:

(1) Thermodynamic modeling can be applied to the systems of cement-stabilized soils by complementing thermodynamic data with the dissolution equations of the soil minerals. This novel method employs pore solution data to quantify the saturation levels of the minerals of interest, thus revealing more insights into the development

of the corresponding chemical reactions. Techniques such as XRD are encouraged to be combined with the novel model in order to comprehensively characterize the compositional minerals since the investigated aqueous species may not be sufficient.

(2) The formation of pozzolanic products grows linearly with the OH^- concentration of the pore solution, while that of cement hydrates is highly correlated to the dissolution equilibrium of $Ca(OH)_2$ and its complexes. The $Ca(OH)_2$ in the pore solution is undersaturated after 5 h due to its consumption by the soil minerals. $CaOH^+$ appears to be the main chemical speciation of the Ca species and participates in the corresponding chemical reactions, with higher saturation levels resulting in higher amounts of cement hydrates.

(3) JA alters the performances of cement-stabilized soils through the dissolution of its compositional minerals. When the pore solution is undersaturated, the proper JA dose improves the OH^- concentration within the pore solution, accelerates the dissolution of the raw materials and increases the saturation of the aqueous species, thereby improving the formation of the reaction products and the compressive strength of the specimen. However, limited by the dissolution equilibrium of $Ca(OH)_2$ and its complexes, the excessively dissolved OH^- from excessive JA doses would inhibit the dissolution of cement clinkers, which would result in the formation of CO_2–containing hydrates and a reduction in the compressive strength.

(4) The $CaOH^+$ saturation is increased by adding PNS since the PNS molecules adsorb preferentially on montmorillonite over the clinkers, thereby lowering the consumption of the Ca species. This behavior accelerates cement hydration but hinders the formation of pozzolanic products. Due to the inevitable adsorption of the clinkers, an excessive PNS addition would lower the acceleration of cement hydration. Nevertheless, the compressive strength of the cement-stabilized soils in the PNS series exceeded that of the plain specimen in this study since cement hydrates are primarily responsible for compressive strength.

Author Contributions: Conceptualization, F.X. and E.J.; methodology, F.X.; software, E.J.; validation, F.X. and E.J.; formal analysis, F.X.; investigation, H.W.; resources, W.Q.; data curation, Y.H.; writing—original draft preparation, F.X.; writing—review and editing, F.X., E.J. and. P.Z.; supervision, W.Q.; funding acquisition, F.X. All authors have read and agreed to the published version of the manuscript.

Funding: This study was funded by the National Natural Science Foundation of China (grant No.: 52109161), the China Postdoctoral Science Foundation (grant No.: 2021M691630) and the National Key R&D Program of China (grant No.: 2021YFB2600704).

Institutional Review Board Statement: Not applicable.

Informed Consent Statement: Not applicable.

Data Availability Statement: Not applicable.

Conflicts of Interest: The authors declare no conflict of interest.

References

1. Sharma, L.K.; Sirdesai, N.N.; Sharma, K.M.; Singh, T.N. Experimental Study to Examine the Independent Roles of Lime and Cement on the Stabilization of a Mountain Soil: A Comparative Study. *Appl. Clay Sci.* **2018**, *152*, 183–195. [CrossRef]
2. Horpibulsuk, S.; Suddeepong, A.; Chinkulkijniwat, A.; Liu, M.D. Strength and Compressibility of Lightweight Cemented Clays. *Appl. Clay Sci.* **2012**, *69*, 11–21. [CrossRef]
3. Xu, F.; Wei, H.; Qian, W.; Cai, Y. Composite Alkaline Activator on Cemented Soil: Multiple Tests and Mechanism Analyses. *Constr. Build. Mater.* **2018**, *188*, 433–443. [CrossRef]
4. Lu, Y.; Liu, S.; Zhang, Y.; Li, Z.; Xu, L. Freeze-Thaw Performance of a Cement-Treated Expansive Soil. *Cold Reg. Sci. Technol.* **2020**, *170*, 102926. [CrossRef]
5. Plank, J.; Sakai, E.; Miao, C.W.; Yu, C.; Hong, J.X. Chemical Admixtures—Chemistry, Applications and Their Impact on Concrete Microstructure and Durability. *Cem. Concr. Res.* **2015**, *78*, 81–99. [CrossRef]
6. Akula, P.; Little, D.N. Coupled Thermodynamic and Experimental Approach to Evaluate Ettringite Formation in a Soil Stabilized with Fluidized Bed Ash By-Product: A Case Study. *Transp. Geotech.* **2020**, *23*, 100352. [CrossRef]

7. Wang, J.; Schweizer, D.; Liu, Q.; Su, A.; Hu, X.; Blum, P. Three-Dimensional Landslide Evolution Model at the Yangtze River. *Eng. Geol.* **2021**, *292*, 106275. [CrossRef]
8. Ge, L.; Wang, C.-C.; Hung, C.-W.; Liao, W.-C.; Zhao, H. Assessment of Strength Development of Slag Cement Stabilized Kaolinite. *Constr. Build. Mater.* **2018**, *184*, 492–501. [CrossRef]
9. Yang, Q.; Du, C.; Zhang, J.; Yang, G. Influence of Silica Fume and Additives on Unconfined Compressive Strength of Cement-Stabilized Marine Soft Clay. *J. Mater. Civ. Eng.* **2020**, *32*, 4019346. [CrossRef]
10. Provis, J.L. Alkali-Activated Materials. *Cem. Concr. Res.* **2018**, *114*, 40–48. [CrossRef]
11. Cristelo, N.; Glendinning, S.; Fernandes, L.; Pinto, A.T. Effect of Calcium Content on Soil Stabilisation with Alkaline Activation. *Constr. Build. Mater.* **2012**, *29*, 167–174. [CrossRef]
12. Sargent, P. The Development of Alkali-Activated Mixtures for Soil Stabilisation. In *Handbook of Alkali-Activated Cements, Mortars and Concretes*; Woodhead Publishing: Sawston, UK, 2015; ISBN 9781782422884.
13. Dong, Y.; Cui, L.; Zhang, X. Multiple-GPU Parallelization of Three-Dimensional Material Point Method Based on Single-Root Complex. *Int. J. Numer. Methods Eng.* **2022**, *123*, 1481–1504. [CrossRef]
14. Jin, L.; Song, W.; Shu, X.; Huang, B. Use of Water Reducer to Enhance the Mechanical and Durability Properties of Cement-Treated Soil. *Constr. Build. Mater.* **2018**, *159*, 690–694. [CrossRef]
15. Xu, F.; Cai, Y.; Qian, W.; Wei, H.; Zhuang, H.; He, Y. Characterization and Mechanism Analysis of Polynaphthalene Sulfonate Modified Cemented Soil. *Constr. Build. Mater.* **2020**, *240*, 117936. [CrossRef]
16. Yan, Z.Y.; Tong, X.D.; Zhou, M.M. Experiment of Cement-Stabilized Soil Mixed High Efficient Naphthalene Water Reducing Agent in Laboratory. *Chin. J. Undergr. Space Eng.* **2009**, *5*, 920–923.
17. Yu, F.; Huang, Y.; Sun, D. Modification Effect of Lime Soil and Cement Soil by Water-Reducing Agent. *J. Build. Mater.* **2017**, *20*, 283–287.
18. Chrysochoou, M. Investigation of the Mineral Dissolution Rate and Strength Development in Stabilized Soils Using Quantitative X-Ray Diffraction. *J. Mater. Civ. Eng.* **2014**, *26*, 288–295. [CrossRef]
19. Lu, Y.; Liu, S.; Zhang, Y.; Wang, L.; Li, Z. Hydraulic Conductivity of Gravelly Soils with Various Coarse Particle Contents Subjected to Freeze–thaw Cycles. *J. Hydrol.* **2021**, *598*, 126302. [CrossRef]
20. Lothenbach, B.; Zajac, M. Application of Thermodynamic Modelling to Hydrated Cements. *Cem. Concr. Res.* **2019**, *123*, 105779. [CrossRef]
21. Scrivener, K.L.; Nonat, A. Hydration of Cementitious Materials, Present and Future. *Cem. Concr. Res.* **2011**, *41*, 651–665. [CrossRef]
22. Rothstein, D.; Thomas, J.J.; Christensen, B.J.; Jennings, H.M. Solubility Behavior of Ca-, S-, Al-, and Si-Bearing Solid Phases in Portland Cement Pore Solutions as a Function of Hydration Time. *Cem. Concr. Res.* **2002**, *32*, 1663–1671. [CrossRef]
23. Zajac, M.; Skocek, J.; Adu-Amankwah, S.; Black, L.; Ben Haha, M. Impact of Microstructure on the Performance of Composite Cements: Why Higher Total Porosity Can Result in Higher Strength. *Cem. Concr. Compos.* **2018**, *90*, 178–192. [CrossRef]
24. Ke, X.; Bernal, S.A.; Provis, J.L.; Lothenbach, B. Thermodynamic Modelling of Phase Evolution in Alkali-Activated Slag Cements Exposed to Carbon Dioxide. *Cem. Concr. Res.* **2020**, *136*, 106158. [CrossRef]
25. Yu, H.; Huang, X.; Ning, J.; Zhu, B.; Cheng, Y. Effect of Cation Exchange Capacity of Soil on Stabilized Soil Strength. *Soils Found.* **2014**, *54*, 1236–1240. [CrossRef]
26. Du, Y.J.; Jiang, N.J.; Liu, S.Y.; Jin, F.; Singh, D.N.; Puppala, A.J. Engineering Properties and Microstructural Characteristics of Cement-Stabilized Zinc-Contaminated Kaolin. *Can. Geotech. J.* **2014**, *51*, 289–302. [CrossRef]
27. Zhao, H.; Liu, J.; Guo, J.; Zhao, C.; Gong, B.W. Reexamination of Lime Stabilization Mechanisms of Expansive Clay. *J. Mater. Civ. Eng.* **2015**, *27*, 4014108. [CrossRef]
28. Parkhurst, D.L.; Appelo, C.A.J. Description of Input and Examples for PHREEQC Version 3—A Computer Program for Speciation, Batch-Reaction, One-Dimensional Transport, and Inverse Geochemical Calculations. In *U.S. Geological Survey Techniques and Methods, Book 6*; U.S. Department of the Interior: Washington, DC, USA; U.S. Geological Survey: Reston, VA, USA, 2013; Chapter 43A.
29. Lothenbach, B.; Kulik, D.A.; Matschei, T.; Balonis, M.; Baquerizo, L.; Dilnesa, B.; Miron, G.D.; Myers, R.J. Cemdata18: A Chemical Thermodynamic Database for Hydrated Portland Cements and Alkali-Activated Materials. *Cem. Concr. Res.* **2019**, *115*, 472–506. [CrossRef]
30. Khorshidi, M.; Lu, N. Intrinsic Relation between Soil Water Retention and Cation Exchange Capacity. *J. Geotech. Geoenviron. Eng.* **2017**, *143*, 4016119. [CrossRef]
31. Zajac, M.; Skocek, J.; Lothenbach, B.; Mohsen, B.H. Late Hydration Kinetics: Indications from Thermodynamic Analysis of Pore Solution Data. *Cem. Concr. Res.* **2020**, *129*, 105975. [CrossRef]
32. Thomas, J.J.; Rothstein, D.; Jennings, H.M.; Christensen, B.J. Effect of Hydration Temperature on the Solubility Behavior of Ca-, S-, Al-, and Si-Bearing Solid Phases in Portland Cement Pastes. *Cem. Concr. Res.* **2003**, *33*, 2037–2047. [CrossRef]
33. Miron, G.D.; Kulik, D.A.; Dmytrieva, S.V.; Wagner, T. GEMSFITS: Code Package for Optimization of Geochemical Model Parameters and Inverse Modeling. *Appl. Geochem.* **2015**, *55*, 28–45. [CrossRef]
34. Rożek, P.; Król, M.; Mozgawa, W. Geopolymer-Zeolite Composites: A Review. *J. Clean. Prod.* **2019**, *230*, 557–579. [CrossRef]
35. Lothenbach, B.; Bernard, E.; Mäder, U. Zeolite Formation in the Presence of Cement Hydrates and Albite. *Phys. Chem. Earth* **2017**, *99*, 77–94. [CrossRef]

36. Tardy, Y.; Duplay, J. A Method of Estimateng the Gibbs Free Energies of Formation of Hydrated and Dehydrated Clay Minerals. *Geochim. Cosmochim. Acta* **1992**, *56*, 3007–3029. [CrossRef]
37. Chen, H.; Feng, P.; Ye, S.; Sun, W. The Coupling Effect of Calcium Concentration and pH on Early Hydration of Cement. *Constr. Build. Mater.* **2018**, *185*, 391–401. [CrossRef]
38. Khalifa, A.Z.; Cizer, Ö.; Pontikes, Y.; Heath, A.; Patureau, P.; Bernal, S.A.; Marsh, A.T.M. Advances in Alkali-Activation of Clay Minerals. *Cem. Concr. Res.* **2020**, *132*, 106050. [CrossRef]
39. Prince, W.; Espagne, M.; Aıtcin, P.C. Ettringite Formation: A Crucial Step in Cement Superplasticizer Compatibility. *Cem. Concr. Res.* **2003**, *33*, 635–641. [CrossRef]
40. Aydin, S.; Hilmi Aytaç, A.; Ramyar, K. Effects of Fineness of Cement on Polynaphthalene Sulfonate Based Superplasticizer-Cement Interaction. *Constr. Build. Mater.* **2009**, *23*, 2402–2408. [CrossRef]
41. Tang, C.S.; Wang, D.Y.; Zhu, C.; Zhou, Q.Y.; Xu, S.K.; Shi, B. Characterizing Drying-Induced Clayey Soil Desiccation Cracking Process Using Electrical Resistivity Method. *Appl. Clay Sci.* **2018**, *152*, 101–112. [CrossRef]
42. Du, J.; Zhou, A.; Lin, X.; Bu, Y.; Kodikara, J. Revealing Expansion Mechanism of Cement-Stabilized Expansive Soil with Different Interlayer Cations through Molecular Dynamics Simulations. *J. Phys. Chem. C* **2020**, *124*, 14672–14684. [CrossRef]
43. Scrivener, K.L.; Juilland, P.; Monteiro, P.J.M. Advances in Understanding Hydration of Portland Cement. *Cem. Concr. Res.* **2015**, *78*, 38–56. [CrossRef]
44. Xu, F.; Wei, H.; Qian, W.; Chen, X.; Xu, T.; He, Y.; Wen, G. Experimental Investigation on Replacing Cement by Sintered Limestone Ash from the Steelmaking Industry for Cement-Stabilized Soil: Engineering Performances and Micro-Scale Analysis. *Constr. Build. Mater.* **2020**, *235*, 117425. [CrossRef]
45. Monteiro, P.J.M.; Geng, G.; Marchon, D.; Li, J.; Alapati, P.; Kurtis, K.E.; Qomi, M.J.A. Advances in Characterizing and Understanding the Microstructure of Cementitious Materials. *Cem. Concr. Res.* **2019**, *124*, 105806. [CrossRef]
46. McDonald, L.J.; Afzal, W.; Glasser, F.P. Evidence of Scawtite and Tilleyite Formation at Ambient Conditions in Hydrated Portland Cement Blended with Freshly-Precipitated Nano-Size Calcium Carbonate to Reduce Greenhouse Gas Emissions. *J. Build. Eng.* **2022**, *48*, 103906. [CrossRef]
47. Zajac, M.; Lechevallier, A.; Durdzinski, P.; Bullerjahn, F.; Skibsted, J.; Ben Haha, M. CO_2 Mineralisation of Portland Cement: Towards Understanding the Mechanisms of Enforced Carbonation. *J. CO_2 Util.* **2020**, *38*, 398–415. [CrossRef]
48. von Greve-Dierfeld, S.; Lothenbach, B.; Vollpracht, A.; Wu, B.; Huet, B.; Andrade, C.; Medina, C.; Thiel, C.; Gruyaert, E.; Vanoutrive, H.; et al. Understanding the Carbonation of Concrete with Supplementary Cementitious Materials: A Critical Review by RILEM TC 281-CCC. *Mater. Struct.* **2020**, *53*, 136. [CrossRef]
49. Hanehara, S.; Yamada, K. Interaction between Cement and Chemical Admixture from the Point of Cement Hydration, Absorption Behaviour of Admixture, and Paste Rheology. *Cem. Concr. Res.* **1999**, *29*, 1159–1165. [CrossRef]